Simultaneous schlieren and shadowgraph visualization of fluid flow using one color CCD camera

A Martinez Gonzalez[1], and D Moreno Hernandez[2]

[1]Depto. de Ingeniería Robótica, Universidad Politécnica del Bicentenario, Carr. Silao - Romita km 2, San Juan de los Duran, C. P. 36283, Silao, Guanajuato, México.

[2]Centro de Investigaciones en Óptica A.C., Loma del Bosque 115, Lomas del Campestre, CP 37150, León, Guanajuato, México.

This article is dedicated to Professor Cesar Sciammarella

Fluid flow analysis, where its behavior is highly unstable, requires information from different optical methods to validate the observables. Usually, this task is carried out by implementing different optical setups, and the visualization of the flow. However, the complexity of these systems makes their implementation a challenge. Therefore, to facilitate the study of this fluid flow phenomenon with more manageable optical systems, we propose a z-schlieren setup that allows simultaneous recording of horizontal and vertical sensitivity schlieren images and shadowgraph images. The optical system employs two ultra-thin filters, an RGB Light Emitting Diode (LED), and a color digital camera. The performance of the optical system is demonstrated by visualizing different fluid flows. The results of this study show that shadowgraph images are contaminated with the crosstalk effect, and correction against it was applied. The data obtained is significantly improved over the existing standard schlieren methods. © Anita Publications. All rights reserved.

1 Introduction

Detailed visualization of the behavior of fluid flows is of great importance in various branches of science [1-10]. Optical techniques are commonly used for their well-known advantages: full field and non-intrusive [11]. The most common optical techniques used to visualize are shadowgraph and schlieren. Both optical methods are easy to implement, low cost, have conventional light sources, and have high and variable sensitivity [12,13].

The shadowgraph method detects displacement of light ray deviation due to changes in the refractive index of the fluid flow represented as shades on the observation plane. On the other hand, a schlieren method detects ray deflection due to refractive index variations. A shadowgraph contains refractive index gradients in the horizontal and vertical directions. However, a schlieren image represents gradients in only one direction; which depends on the knife edge's orientation in the optical system. Therefore, a schlieren system does not deliver complete information on the fluid flow under analysis. Several works have been proposed to alleviate this disadvantage using different optical setups [18-25]. But most of the optical systems developed are complex since they require complicated alignments due to the number of components and also may be costly [18-22]. In some methods, the optical arrangement is simple, but the approach needs to care about

---

Corresponding author

e mail: amartinezg@upbicentenario.edu (A Martinez Gonzalez); *dmh@cio.mx* (D Moreno Hernandez)

diffraction effects since resolution may be compromised due to the size of the source filter and aperture [23]. Another simple and inexpensive work uses two filters centered on red and blue colors placed at right angles to obtain refractive index gradients in both directions [24]. But the optical system uses a halogen lamp in which the sensor receives a broad-spectrum illumination, and some wavelengths are not filtered. In this approach, the filters were made by trial and error, and the light source aperture comprises two crossed slits so that diffraction effects may occur. All these optical system characteristics could compromise image quality. In other studies, the refractive index gradients are determined by relating ray deflection to color attribute variations (hue intensities) of the schlieren images [25].

However, none of these optical systems were used to simultaneously determine the displacement and deflection of light rays. Nevertheless, there is a reported work where the displacement and deflection of light rays are simultaneously detected using the shadowgraph and schlieren methods, but the optical system used represents a challenge for its implementation [26]. And the optical system that detects schlieren images is sensitive only in one direction. The development of a simple optical system that simultaneously obtain shadowgraph and schlieren images was recently reported [27]. Also, in this work, the optical system allows obtaining sensitive schlieren images in the horizontal and vertical directions. However, the shadowgraph images obtained with this optical setup are contaminated with the crosstalk effect because the schlieren and shadowgraph images are recorded simultaneously in an RGB digital camera. However, most digital color camera sensors have overlapping sensibilies, known as the crosstalk effect, that distorts the recorded data, forcing compensation algorithms to use [28]. Therefore, the optical setup implemented in this work is a z-schlieren arrangement with two independent knife edges in the same beam path. The knife edges correspond to shortpass and longpass ultra-thin filters [29]. The filters enhance vertical and horizontal refractive index variations in schlieren images. However, crosstalk distortion present in the schlieren and shadowgraph images needs to be compensated to improve the performance of the optical system.

2 Shadowgraph and schlieren techniques

The optical methods sensitive to fluid flow density variations studied in this work are the schlieren and shadowgraph methods. In these optical techniques, we assume that the density and the refractive index of the fluid are linearly related through the Gladstone-Dale equation [12]:

$$(n - 1) = K\rho \tag{1}$$

where ρ and n are the density and the refractive index of the gas, and K is the Gladstone-Dale's constant. The Gladstone-Dale's constant is a function of both the wavelength of light source and the physical properties of gas [16]. Each technique registers only one variable in the observation plane, i.e., light ray displacement and deflection for shadowgraph and schlieren, respectively, and each of these optical systems has its own elements for its implementation.

Shadowgraph method

In the shadowgraph method, light rays that are displaced due to density changes in the fluid flow manifest as intensity variations represented as shades on the observation plane. Moreover, these intensity variations are proportional to the second derivative of the density [16,17]:

$$\frac{\Delta I}{I} \approx lK \int_0^L \left(\frac{\partial^2 \rho}{\partial^2 x} + \frac{\partial^2 \rho}{\partial^2 y} \right) dz \tag{2}$$

where I is light intensity, x and y are cartesian coordinates perpendicular to ray propagation, and L and l represent the width and position of the object under test. The system's sensitivity can be manipulated by changing the value of the object's position under analysis.

Schlieren method

In schlieren visualization, the integral flow properties along a given ray's optical path contribute to the light intensity at the observation plane. In a classical Schlieren system, the light from the source is collimated by a primary lens. After the collimated beam passes through the test section, it is refocused by a second lens. A knife-edge is then placed at this focal point, which is the exit focal point of the system. When the knife-edge is placed horizontally, positive density gradients are visualized as light areas and negative gradients as dark ones. This behavior is because light rays deflected upwards by the positive gradients miss the knife-edge, whereas the knife blocks out those deflected downwards by the negative gradients. A detailed description of the schlieren technique can be found in [16,17]. The focal distance of the second lens and the position of the cutoff device with respect to the image of the light source determines the sensitivity of a schlieren optical setup (see Fig 1).

The density gradient in a typical schlieren method is obtained in only one direction; it depends on the orientation of the knife edge at the focal point of the second lens. That is, its magnitude is determined in a predetermined direction, such as:

$$\rho_x = \frac{\partial \rho}{\partial x} \text{ or } \qquad \rho_y = \frac{\partial \rho}{\partial y} \tag{3}$$

In this way, it is necessary to change the classic schlieren system to have an optical system with sensitivity in the horizontal and vertical directions.

3 Cross talk correction

An image given by RGB digital camera can be separated into three different color channels and each channel corresponds to red, green, and blue colors, respectively. Hence, each color channel provides specific information about the object under analysis. Since color digital cameras are usually configured according to Bayer mosaic filtered color, the green color channel is more sensitive than the other two color channels. The intensity value in each color channel can be approximated in a matrix form in the following way [25]:

$$\hat{I} = \sum_{j=0}^{2} A_{ij} I_j \tag{4}$$

where A_{ij} represents the crosstalk effect of a digital color camera and stands for the calibration coefficients relating spectral pixel response to specific incident illumination response. The subscript i stands for each color channel and j for the color illumination source. In other words, the intensities $\hat{I}_i$ are the intensities projected on the red, green, and blue color channels. However, the numerical values of the light intensities $\hat{I}_j$ in Eq (4) are not explicitly known and must be determined by solving Eq (4). Therefore, Eq (4) can be represented in expanded form as:

$$\hat{I}_R = A_{Rr} I_r + A_{Rg} I_g + A_{Rb} I_b \tag{5a}$$

$$\hat{I}_G = A_{Gr} I_r + A_{Gg} I_g + A_{Gb} I_b \tag{5b}$$

$$\hat{I}_B = A_{Br} I_r + A_{Gg} I_g + A_{Bb} I_b \tag{5c}$$

The coefficients A can be calculated by relating the spectral response of the digital camera's pixels to the spectral response of a specific incident light on the pixels. Equation (5) can be represented in matrix form in the following way:

$$\begin{bmatrix} \hat{I}_R \\ \hat{I}_G \\ \hat{I}_B \end{bmatrix} = \begin{bmatrix} A_{Rr} & A_{Rg} & A_{Rb} \\ A_{Gr} & A_{Gg} & A_{Gb} \\ A_{Br} & A_{Gg} & A_{Bb} \end{bmatrix} \begin{bmatrix} I_r \\ I_g \\ I_b \end{bmatrix} \tag{6}$$

Finally, the solution of Eq (6) is required to obtain the intensity values of the color illumination source incident on the color digital camera.

4 Experimental setup

The optical setup consists of two spherical mirrors of focal distance *f* =1.54 m, an illumination *rgb* Light Emitting Diode (LED), an ultra-thin shortpass filter, an ultra-thin longpass filter, and an *RGB* color digital camera (see Fig 1). The lamp illumination is composed of an *rgb* Plastic Lead Chip Carrier (PLCC) WS2812B manufactured by Worldsemi. The *rgb* PLCC is a smart Light Emitted Diode (LED) source that includes the control and *rgb* chip in one package, allowing each LED to be addressable. The schlieren and shadowgraph images are recorded in an Lt225c model color digital camera provided by Lumenera Corporation. This camera has a 2.2 Megapixel CMOS sensor with a 5.5 µm pixel size.
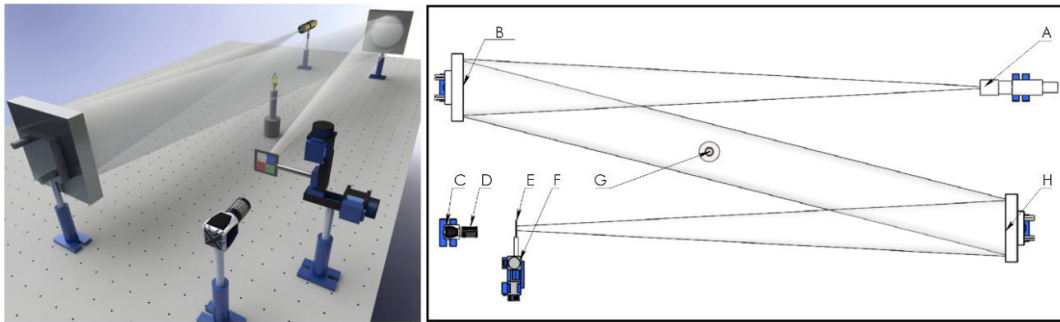

Fig 1. Scheme of horizontal-vertical sensitivity schlieren system and shadowgraph. A-*rgb* LED, BH-Mirrors, C-Camera, D-Navitar Lens, EF-Shortpass and longpass filters, F-Motorized translation stage, G-Test area.
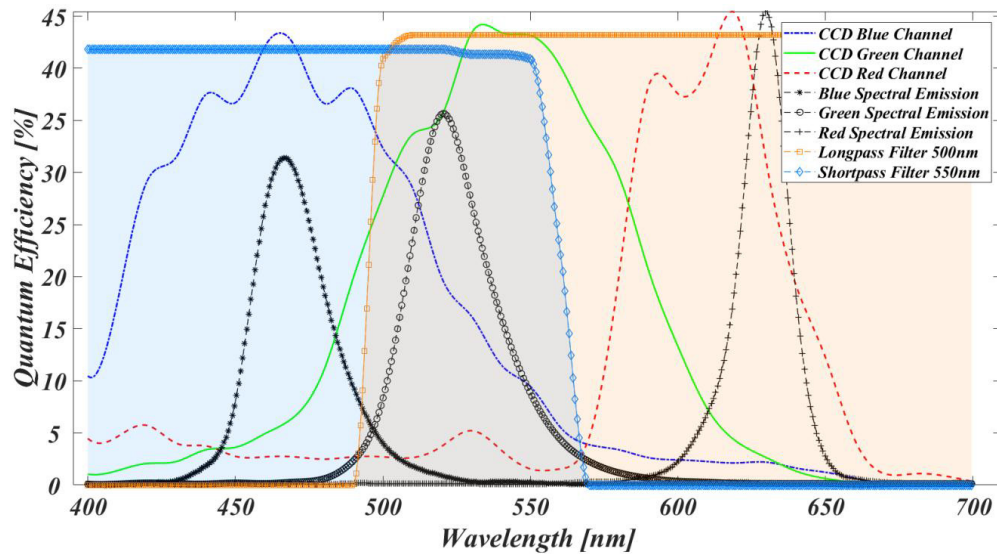

Fig 2. Relation between the spectral responses of the color digital camera, rgb LED, and shortpass and longpass filters.

The light emitted by the *rgb* LED first passes through a lens and a pinhole located at the focal point of the primary spherical mirror. Then, the collimated light coming from the primary spherical mirror illuminates a secondary spherical mirror, which is focused on the second mirror's focus. The two ultra-thin filters are located at this focal point. Each filter allows approximately 50% of the light that falls on it to

pass through. The shortpass and longpass filters are placed at the focus point horizontally and vertically, respectively. Finally, the object under analysis is imaged on a color digital camera using a 50 mm F/2.8 2/3" Navitar lens.

The spectral response of pixels of the digital camera provided by the manufacturer used in this work is shown in Fig 2 [26]. Also, Fig 2 depicts the spectral response of the shortpass and longpass filters and the spectral response of the *rgb* illumination [24]. The spectral response of the *rgb* LED is determined by using a mini-spectrometer HR4000 of Ocean Optics. Figure 2 shows that the *rgb* PLCC spectrum is composed of three peaks corresponding to red, green, and blue colors and shows the overlap of the *RGB* color digital camera spectra and the *rgb* LED light spectra. This overlapping shows the crosstalk effect and is present in color digital cameras. We can note that this crosstalk effect is more intense on the green and blue color channels than on the red color channel. Therefore, it is necessary to correct this effect to improve the quality of the schlieren and shadowgraph images.

The tests are achieved by visualizing the convective fluid flow generated by a heated Rectangular Metal Plate (RP), the hot air releasing from a 13 mm circular nozzle (CN), and the flame of two Pencil Soldering Iron (PSI) in angle.

The RP (7.3 cm×11 cm) used in this work corresponds to a programmable chilling/heating plate provided by Torrey Pines Scientific. The programmable plate allows us to induce plate temperatures on the surface from −10°C to 100°C. The test was performed at a temperature of 100 °C.

The hot air is generated in a soldering station welding with a nozzle containing a swirl chamber to release uniform hot air. This equipment includes a display to select the desired temperature value, and it is possible to choose values from 100 °C up to 600 °C. The test was carried out with an air temperature shown at the display of 350°C

The torch head of the PSI used in this experiment has an axisymmetric cylindrical configuration with inner and outer diameters of 2 mm and 8 mm, respectively. The torch has four slots that admit air into the stream via the Venturi effect to ensure a proper air/fuel mixture for relatively hot flames, and it uses butane gas for its operation.

5 Experimental Results

In this work, the convective flow generated by a heated RP, the hot air of a CN, and the flame of two PSI in angle are visualized to test the optical system presented here. But first, we explain the functioning of the ultrathin filters. For example, in Fig 2, the shortpass filter blocks the red light, so the filter blocks 50% of the red light, and the rest goes directly to the red channel of the digital camera. In the same way, the longpass filter blocks 50% of the blue light, and the rest goes directly to the blue channel of the digital camera. Then, the schlieren images are recorded from the shortpass and longpass filters in the red and blue color channels, respectively. However, as we can see, the green light is not blocked by any of the two filters, so the green light is recorded in the green channel, and this information corresponds to shadowgraph images. Therefore, the optical system presented in this work record simultaneously schlieren images sensitive to horizontal and vertical directions and shadowgraph images in one snapshot.

To improve shadowgraph and schlieren image quality is needed to correct it against the crosstalk effect. The crosstalk coefficients can be determined in different ways; one way is directly from the overlapping between spectral intensity values of the color illumination source (*rgb* LED) and the spectral response on each digital camera pixel (see Fig 2). However, we opt for an experimental method to determine the crosstalk coefficients. The procedure consisted of directly illuminating the digital camera with each color of the LED. For each case, an image was recorded. Then, the contribution of each illumination color in each color channel of the camera was determined. The crosstalk coefficients correspond to the average intensity of each image

color channel. Before calculating the crosstalk coefficients, the intensity of each LED color was equalized. The values obtained with this procedure were: $A_{Rr} = 6.55 \times 10^4$, $A_{Rg} = 0$, $A_{Rb} = 0$, $A_{Gr} = 0.26 \times 10^4$, $A_{Gg} = 5.78 \times 10^4$, $A_{Gb} = 2.31 \times 10^4$, $A_{Br} = 0$, $A_{Bg} = 0$, and $A_{Bb} = 6.55 \times 10^4$. Once the crosstalk coefficients are known, the solution of Eq (6) is straightforward. These crosstalk coefficients are used to solve Eq (6) to obtain the values of I_r, I_g, and I_b.
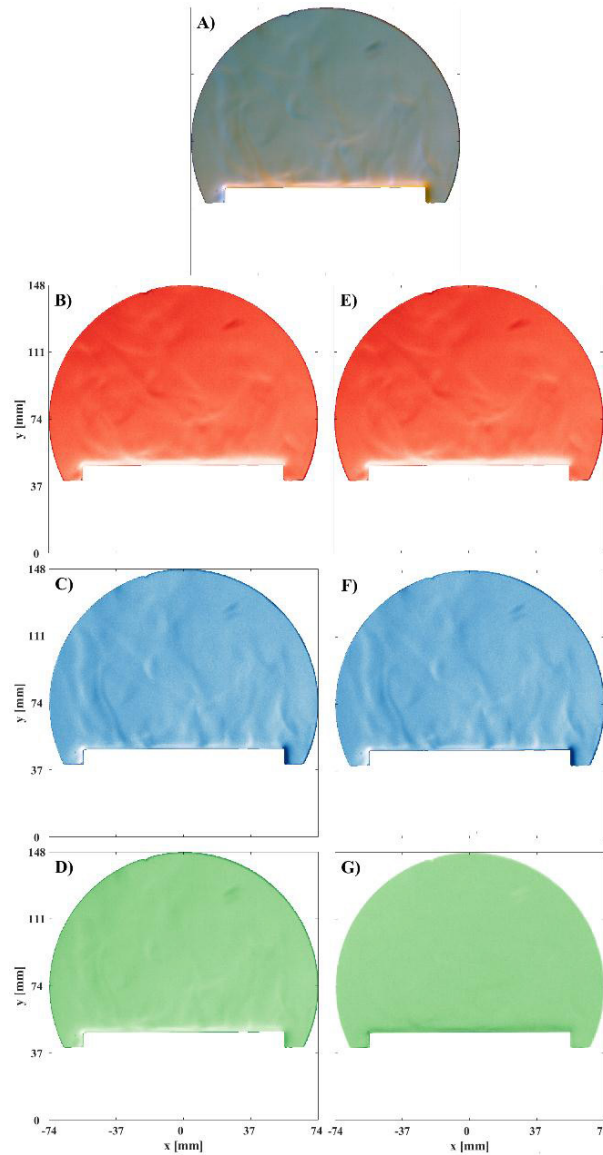
Fig 3. The convective fluid flow of the heated RP. (A) RGB image. (B) Uncorrected horizontal sensitivity schlieren image, (C) Uncorrected vertical sensitivity schlieren image, (D) Uncorrected shadowgraph image. (E) Corrected horizontal sensitivity schlieren image, (F) Corrected vertical sensitivity schlieren image, (G) Corrected shadowgraph image.

Figure 3 shows the digital camera's image of each color channel of the convective fluid flow generated by the heated RP. Separating the images of each color channel, we can appreciate the contribution

of both Schlieren images. Also, the shadowgraph image depicts components of the schlieren effect. Therefore, image correction is applied by solving Eq (6). The result of applying crosstalk correction can be seen in the shadowgraph image; the schlieren contribution was eliminated, remaining only the shades. On the other hand, the horizontal and vertical sensitive schlieren images remain almost unchanged after applying the crosstalk correction. This last result is supported by what is shown in Fig 2, where the crosstalk occurs mainly in the green channel.
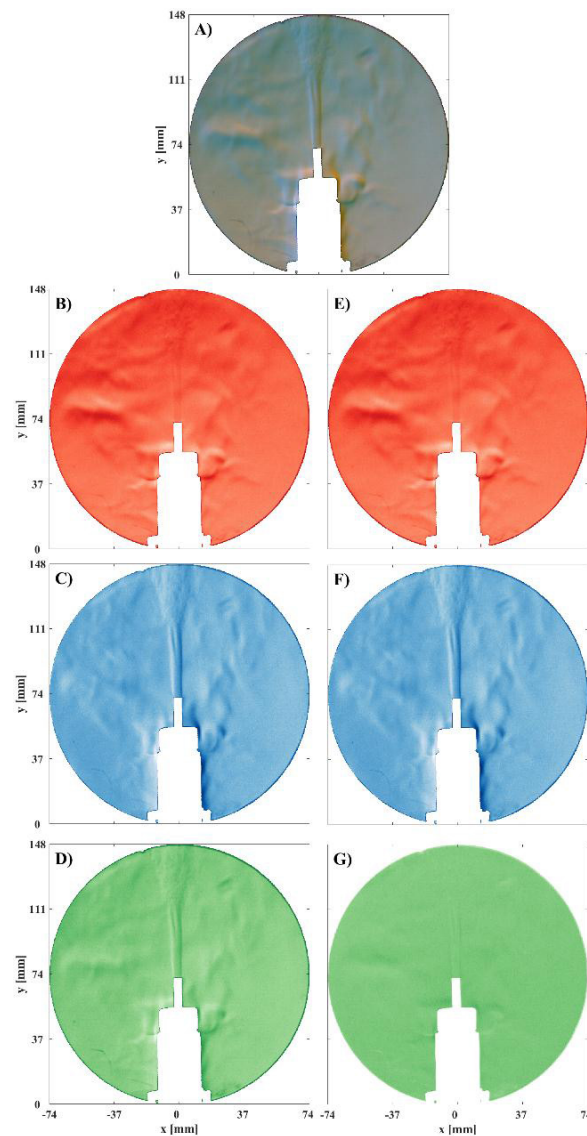

Fig 4. Heated air of the CN. A) RGB image. B) Uncorrected horizontal sensitivity schlieren image, C) Uncorrected vertical sensitivity Schlieren image, D) Uncorrected shadowgraph image. E) Corrected horizontal sensitivity Schlieren image, F) Corrected vertical sensitivity Schlieren image, G) Corrected shadowgraph image.

The fluid flow generated by the CN and the PSI in angle is shown in Figs 4 and 5, respectively. We can note the details of the fluid flow in the pictures in the three cases analyzed. Observe that each of

the schlieren images complements the other. For example, in the regions where there are shadows, in its complementary image, it appears illuminated. In this way, with these two schlieren images, it is possible to obtain more information on the fluid flow studied. On the other hand, the shades of the shadowgraph images of the three cases under study are visible for the flow generated in the CN and PSI. However, the flow generated in the heated RP is barely visible because the sensitivity of the shadowgraph system is lower than that of the schlieren. Then, the shadowgraph system cannot resolve variations of the refractive index corresponding to the temperature values of this flow. However, the optical setup permits determining an angular deflection of 26 µrad [22].
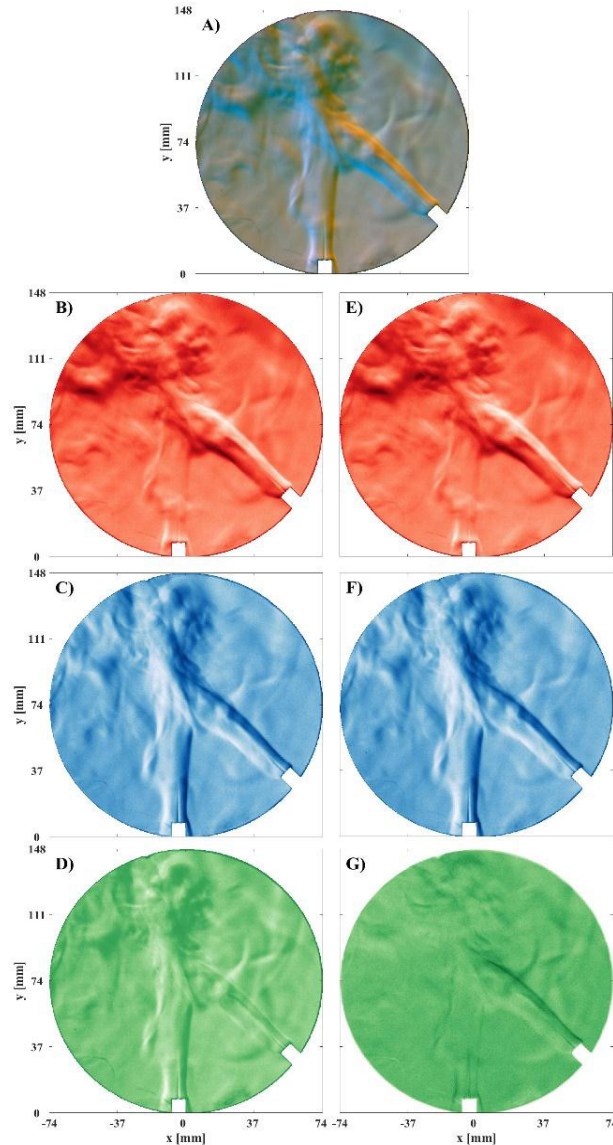

Fig 5. Flame of the PSI. (A) RGB image. (B) Uncorrected horizontal sensitivity schlieren image, (C) Uncorrected vertical sensitivity schlieren image, (D) Uncorrected shadowgraph image. (E) Corrected horizontal sensitivity schlieren image, (F) Corrected vertical sensitivity schlieren image, (G) Corrected shadowgraph image.

6 Conclusions

We presented a method to visualize density variations in fluid flows. A schlieren setup was used for such a purpose. The optical system allows obtaining horizontal y vertical sensitivity schlieren and shadowgraph images simultaneously. The results show that shadowgraph images have low sensitivity due to the inherent characteristics of the optical system. The advantage of the new approach lies in obtaining horizontal and vertical sensitive schlieren and shadowgraph images in a single snapshot. With this, it is possible to unite the characteristics that are not visualized with the standard schlieren arrangement, resulting in improved visualization

Acknowledgments

References

1. Vogel A, Apitz I, Freidank S, Dijkink R, Sensitive high-resolution white-light Schlieren technique with a large dynamic range for the investigation of ablation dynamics, *Opt Lett*, 31(2006)1812–1814.

2. Tang J W, Liebner T J, Craven B A, Settles G S, A schlieren optical study of the human cough with and without wearing masks for aerosol infection control, *J R Soc Interface*, 6(2009)S727–S736.

3. Barnes N F, Bellinger S L, Schlieren and shadowgraph equipment for air flow analysis, *J Opt Soc Am*, 35(1945) 497–509.

4. Korpel A, Yu T T, Snyder H S, Chen Y M, Diffraction-free nature of Schlieren sound-field images in isotropic media, *J Opt Soc Am*, 11(1994)2657–2663.

5. Stanic S, Quantitative schlieren visualization, *Appl Opt*, 17(1978)837–842.

6. Agrawal A K, Butuk N K, Gollahalli S R, Griffin D, Three-dimensional rainbow schlieren tomography of a temperature field in gas flows, *Appl Opt*, 37(1998)479–485.

7. Wong T, Agrawal A K, Quantitative measurements in an unsteady flame using high-speed rainbow schlieren deflectometry, *Meas Sci Technol*, 17(2006)1503; doi. 10.1088/0957-0233/17/6/031.

8. Alvarez-Herrera C, Moreno-Hernández D, Barrientos-García B, Guerrero-Viramontes J A, Temperature measurement of air convection using a Schlieren system, *Opt Laser Technol*, 41(2009)233–240.

9. Martínez-González A, Moreno-Hernández D, León-Rodríguez M, Carrillo-Delgado C, Wide-range average temperature measurements of convective fluid flows by using a schlieren system, *Appl Opt*, 55(2016)556–564.

10. Prevosto L, Artana G, Mancinelli B, Kelly H, Schlieren technique applied to the arc temperature measurement in a high energy density cutting torch, *J Appl Phys*, 107(2010)023304; doi.org/10.1063/1.3291099.

11. Agrež V, Požar T, High-speed photography of shock waves with an adaptive illumination, *Opt Lett*, 45(2020) 1547–1550.

12. Xiao G, Yin J, Chen C, Feng B, Zhong W, Zhang Y, Duan X, Flow visualization and density measurement of the supersonic molecular beam for fusion plasma fueling, *Rev Sci Instrum*, 92(2021)043539; doi.org/10.1063/5.0039181.

13. Underwood T C, Loebner K T, Miller V A, Cappelli M A, Schlieren diagnostic for cinematic visualization of dense plasma jets at Alfvénic timescales, Exp Fluids, 61(2020)1–13.

14. Zhang P, Xu Z, Wang T, Che Z, A method to measure vapor concentration of droplet evaporation based on background oriented Schlieren, *Int J Heat Mass Transfer*, 168(2021)120880; doi.org/10.1016/j.ijheatmasstransfer.2020.120880.

15. Tropea C, Yarin A, Foss J, Handbook of experimental fluid mechanics, (Springer, Berlin), 2007.

16. Merzkirch W, Flow visualization, (Academic Press, Orlando), 1987.

17. Settles G S, Schlieren and shadowgraph techniques, (Springer, Berlin), 2001.

18. Barry F W, Edelman G M, An improved schlieren apparatus, *J Aeronaut Sci*, 15(1948)364; doi.org/10.2514/8.11588.

19. Rudinger G, Somers L M, A Simple Schlieren System for Two Simultaneous Views of a Gas Flow, *J SMPTE*, 66(1957)622; doi: 10.5594/J17005.

20. Owen R B, Witherow W K, United States Patent #4,391,518 (1983).

21. Golub V V, Kharitonov A I, Sharov I L, Shulmeister A M, in Flow Visualization V: Proceedings of the Fifth International Symposium, R. Reznicek, ed, (Taylor and Francis), 1990, p 556.

22. Chaloupka J L, Wood M, Aas J, Hutchins J, Thistle J D, Color schlieren imaging with a two-path, double knife edge system, *Opt Express*, 22(2014)8041–8046.

23. Settles G S, A direction-indicating color schlieren system, *AIAA J*, 8(1970)2282; doi.org/10.2514/3.6106.

24. Stricker J, Zakharin B, Hornick B T, Rosenblatt F, Bidirectional quantitative color schlieren, *Opt Eng*, 45(2006)123604; doi.org/10.1117/1.2402103.

25. Elsinga G E, Oudheusden B W Van, Scarano F, Assessment and application of quantitative schlieren methods: Calibrated color schlieren and background oriented schlieren, *Exp Fluids*, 36(2004) 309–325.

26. Kleine H, Grönig H, Takayama K, Simultaneous Shadow, Schlieren and Interferometric Visualization of Compressible Flows, *Opt Lasers Eng*, 44(2006)170–189.

27. Martinez-Gonzalez A, Moreno-Hernandez D, Horizontally and vertically sensitive schlieren and shadowgraph system, *Opt Lett*, 47(2022)3596–3599.

28. Caspi D, Kiryati N, Shamir J, Range imaging with adaptive color structured light, *IEEE Transactions on Pattern Anal and Mach Intell*, 20(1998)470–480.

29. Edmund Optics: longpass and shortpass optical filters: https://www.edmundoptics.com/f/everix-ultra-thin-shortpass-filters/39542/

30. Lumenera corporation: Lt225 Datasheet, available from: https://www.lumenera.com/lt225.html

Dr Adrian Martínez González obtained his bachelor's degree in Electronics Engineering in 2005 from Instituto Tecnológico de Orizaba, and his Master's degree in Digital Systems in 2007. He obtained his Ph D in Optics in 2014 at Centro de Investigaciones en Óptica. He is a Full-Time Professor at Universidad Politecnica Bicentenario in the Robotics Department, where his research is focused on actuators and sensors in robotics with optical technology and schlieren systems.

Dr David Moreno-Hernández is a researcher at the Center for Research in Optics (CIO) in Mexico. Prior joining to CIO as a researcher, he was in a two-year postdoctoral position at the Fluid Mechanics Research Laboratory (FMRL) of the mechanical engineering department at Florida State University. The research interests of Dr David Moreno-Hernández include the development of optical instrumentation applied to fluid flow analysis.